Chinese Science Bulletin

Flow characteristics and reaction properties of carbon dioxide in microtubules and porous media

ZHAO RenBao[1,2†], YUE XiangAn[1,2], WU YaHong[1], XU ShaoLiang[1], WANG Fei[1] & HOU YongLi[1]

[1] MOE Key Laboratory of Petroleum Engineering, China University of Petroleum, Beijing 102249, China;
[2] Enhanced Oil Recovering Research Center, China University of Petroleum, Beijing 102249, China

Carbon dioxide reacts with porous media while flowing through them enhancing their permeability. Its flow behavior as well as the permeability enhancement effects were studied in synthetic cores, natural cores and microtubes with an inner diameter of 5 μm. The results show that the permeability of H_2O-saturated cores (containing carbonate ingredients) was enhanced by increasing the injection volume of a CO_2-H_2O solution. This enhancement is attributable to carbon dioxide's corrosion, which is justified by SEM scanning. The same phenomenon occurs with a CO_2-H_2O solution in microtubes, but for a different reason. The gas flow velocity of carbon dioxide in microtubes was approximately 100% faster than that of nitrogen because of the scale and the squeezing effects. Carbon dioxide molecules dissolved in water accelerate the diffusion rate of water molecules within the boundary layer, which in turn diminishes the thickness of the water film and enlarges the effective pore size. This flow behavior facilitates the injection of carbon dioxide into low-permeability reservoirs for oil-displacement and formation energy buildup purposes. This behavior also increases the potential for carbon dioxide channeling or release from the formation.

carbon dioxide, enhanced oil recovery, microtubes, microscale effect, corrosion, permeability

As a primary component of greenhouse gases, carbon dioxide has contributed to global environmental degradation. Therefore, an effective way of injecting carbon dioxide into oil reservoirs would not only enhance oil recovery, but also reduce potentially harmful carbon dioxide emissions.

Earlier studies[1] indicated that injected carbon dioxide could result in oil swelling and reduction in oil viscosity, increase reservoir pressure and have a positive influence on dissolved-gas drive and injectivity. However, the few existing research approaches were primarily mechanism studies conducted through such experiments as the corrosion reaction of the CO_2-H_2O solution with cores, core flow tests and the interfacial tension determination of water, oil and carbon dioxide[2,3].

After being injected, carbon dioxide reacts with formation water, oil and rock, thereby changing their percolation behavior. In the process of injecting displacement fluids, flow velocity is dependent on dynamic dispersion and molecular diffusion[4]. However, due to core's complex porous structure, the statistical and macroscopic results from the core flow experiment and some corresponding concepts such as starting pressure gradient[5−7] and wall fluids are unable to provide a quantitative explanation for its flow behavior. Thus the physical and chemical nature of some fluid flow phenomena for nonlinear processes in low permeability reservoirs is not derived from traditional macroscopic and statistic methods. This causes inconsistent results influenced by such factors as the influence of adsorption layers on fluid seepage characteristics[8−10], the differences between the solid-liquid interface and the bulk phase[11,12], and the influence of residual water saturation on the gas slippage effect[13,14].

Received February 25, 2008; accepted May 9, 2008
doi: 10.1007/s11434-008-0456-5
†Corresponding author (email: zhaorenbao@vip.sina.com; zhaorb@cup.edu.cn)
Supported by the "973" Project from the Ministry of Science and Technology of China (Grant No. 2006CB705805) and the National Key Technology R&D Program (Grant Nos. 2006BAB03B06 & 2007BAB17B0B)

Using microtubes[15,16] for investigating the influences of wall fluids simplifies several factors which core flow experiments might omit, such as the fluids flow space, influences of flow direction on mass transfer and chemical reactions between fluids and walls. Quantitative results are obtainable through a combination of two methods for explaining the microscale effect and its influence on the flow behavior of CO_2 and its aqueous solutions.

1 Experimental equipment and techniques

1.1 Experimental facilities and materials

Core flow experimental equipment consists of a constant-flux pump, a manual operated piston screw pump, a piston container and a high pressure vision window. The microflow experimental apparatus is depicted in Figure 1. N_2 or CO_2 from a compressed gas tank flows through the flow control valve into a pressure-buffering reservoir before entering the connective tube linked with the starting point of the microtube connection. The measuring pipe is connected to the microtube on the other end.

Experimental materials: Ultra-pure H_2O, purpose-built synthetic core PC-1, natural core 18-8-1 (from the Changqing Oilfield, Shanxi Province, China), 1 wt% KCl solution, 1 wt % NaCl solution, Silica Glass microtubes. ICP-OES (PerkinElmer, Inc. USA), a scanning electron microscope (SEM, OxfordS-360, England), an X-ray diffractometer (XRD, D/max-2500, Japan).

1.2 Fundamental core sample parameters

Core nitrogen gas permeability was measured after being deoiled and dried, as shown in Tables 1 and 2. The cores described above were all saturated with NaCl saline water prior to use.

Table 1 Data of natural core 18-8-1

Length (cm)	5.21	Diameter (cm)	2.50
Sectional area (cm^2)	4.91	Volume (cm^3)	25.58
Pore volume (cm^3)	4.41	Porosity (%)	17.24
Klinkenberg permeability (N_2)×10^{-3} (μm^2)	0.35	Experimental fluids	solutions of CO_2, KCl, and NaCl

Table 2 Data of synthetic core PC-1

Length (cm)	7.92	Diameter (cm)	2.50
Sectional area (cm^2)	4.91	Volume (cm^3)	38.89
Pore volume (cm^3)	6.09	Porosity (%)	15.65
Klinkenberg permeability (N_2)×10^{-3} (μm^2)	0.28	Experimental fluids	solutions of CO_2, KCl, and NaCl

The cores described above were all saturated with NaCl saline water before use.

1.3 Preparation of CO_2 saturated solutions

CO_2 was injected into a 500 mL acid-proof piston container until the pressure rose to 0.25 MPa, then 1% KCl solution was injected. CO_2 was subsequently injected until the inside pressure reached 1.5—1.9 MPa. During the injection period, the gas-liquid interface was observed through a high pressure vision window. After 24 h, the container was examined to verify it was leak free, with a fully saturated CO_2 solution. The valve was slowly opened and the connected pump was simultaneously turned on to maintain gas-liquid interface stability, guaranteeing that the displacement fluid flowing into the cores was constantly saline water saturated with CO_2 under pressure, with gas prevented from entering.

1.4 Experimental procedure and methodology

The microflow experimental equipment was nearly identical to that described in literature[16] except that one more water column was added in the measuring tube of the flow-meter. The core displacement apparatus was also presented[17] for core flooding experiments.

For porous media, gas permeability was calculated according to the following equation:

$$K_g = \frac{20 p_{sc} Q_{sc} \mu L}{A(p_1^2 - p_2^2)}. \quad (1)$$

Liquid permeability was calculated according to Darcy's formula:

$$K = \frac{10 Q \mu L}{A \Delta P}. \quad (2)$$

In microtubes, the gas and liquid permeability was also calculated according to the above equations, and in addition, it also followed:

$$R_e = \frac{\rho D v}{\mu}, \quad (3)$$

where p_{sc} is the standard atmosphere pressure (MPa), p_1 and p_2 are the inlet and outlet pressure respectively (MPa), Q_{sc} is the gas volume flow rate under p_{sc} (cm^3/s), L is the length of the rock sample (cm), μ is the viscosity (mPa·s), K is the permeability (μm^2), A is the cross-sectional area (cm^2), D is the inside diameter of microtubes (m), ρ is the fluid density (kg/m^3) and v is the flow velocity (m/s). At the experiment temperature, viscosity of N_2 is 0.0178 mPa·s and CO_2 is 0.0151 mPa·s.

2 Results

2.1 CO_2 flow in microtubes

The reservoir was not filled water and directly connected to the measurement system and the gas filter system which measured the gas flow rate. Two small water slugs divided by an air slug were injected into the 1mm diameter measurement pipe (Figure 1). When N_2 was employed as the injection fluid, the two interfaces between the water and the air slug moved with the same rate because of the poor solubility of N_2 in water. However, this was not also the case for CO_2. With the increase of injection pressure at the microtube inlets, the velocity of the two interfaces increased. Because CO_2 dissolved in and was transported through the left water plug into the air slug, the volume of the air slug increased and thus increased the velocity of interface 2. Therefore, the volume of the air slug increased in the process of measurement because of CO_2 diffusion in water.

CO_2 flowed faster than N_2 in microtubes under the same pressure gradient as shown in Figure 2(a). The difference of the flow velocity became greater with the pressure gradient increase.

The relative permeability of CO_2 in microtubes, which was calculated according to equation 1, was almost twice that of N_2 under the same average pressure as shown in Figure 2(b). The relative permeability of both gases decreased with the increase of pressure.

Because neither CO_2 nor N_2 reacted with the microtubes, a larger relative CO_2 permeability was attributed to the lower viscosity of CO_2 and scaling effects after eliminating the disturbance factors of the corrosion reaction.

2.2 Flow behavior of the CO_2 solution in microtubes

The reservoir was filled with distilled water (shown in Figure 1) which was subsequently respectively displaced by N_2 and CO_2. As shown in Figure 3(a), the flow velocities of gas displaced water in the microtube were different under the same pressure gradient. The flow velocity of the water displaced by CO_2 at a low pressure gradient moved more slowly than that of water displaced by N_2, but with the increase of the pressure gradient, the former increased more rapidly than the latter, eventually exceeding it when the pressure gradient reached approximately 25 MPa/m. As shown in Figure 3(b), the relative permeability of water displaced by CO_2 increased more rapidly than that of water displaced by N_2.

As shown in Figure 4, the Reynolds numbers of distilled water flowing in microtubes which was displaced by CO_2 and N_2 were different. Under a low pressure gradient, the Reynolds number of water which was displaced by CO_2 was smaller than that of water displaced

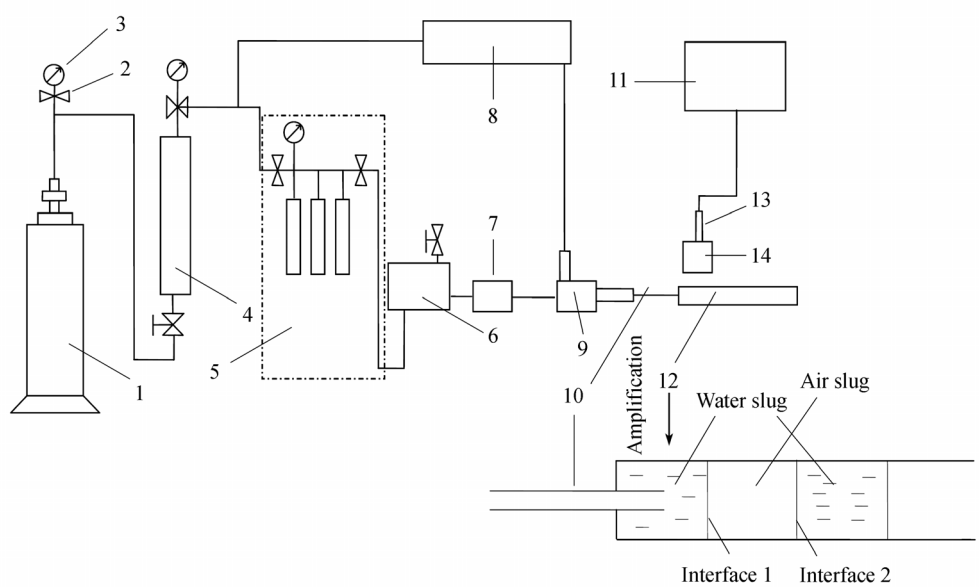

Figure 1 Experimental apparatus: 1, Compressed N_2 (CO_2) tank; 2, pressure gauge; 3, valve; 4, pressure-buffering reservoir; 5, gas filter; 6, liquid reservoir; 7, liquid filter; 8, pressure and temperature sensor; 9, three-way pipe; 10, microtubes; 11, computer; 12, measuring pipe; 13, real-time image acquisition system; 14, microscope.

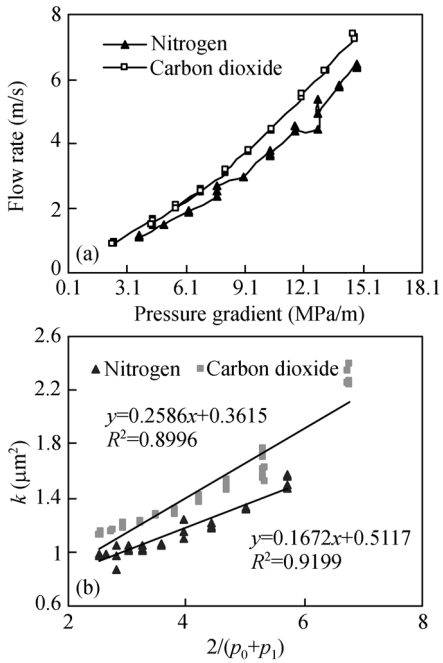

Figure 2 (a) Influence of injection pressure on fluid velocity; (b) influence of average pressure on relative permeability.

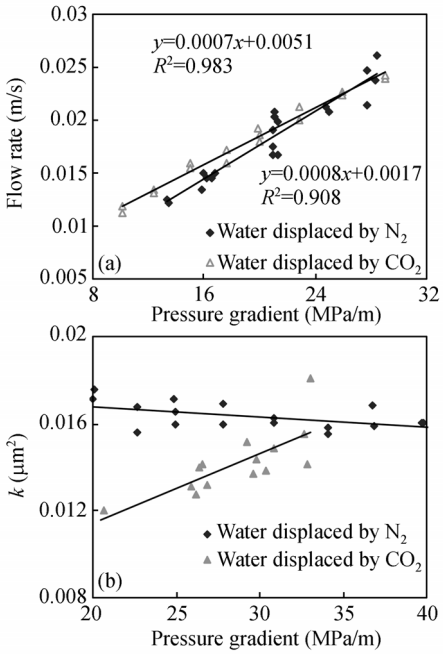

Figure 3 (a) Flow rate changes with different pressure gradients; (b) water relative permeability in microtubes changes with different gas displaced.

by N_2. However, with the increase of pressure gradient, the Reynolds number of water displaced by CO_2 increased more rapidly than that of water displaced by N_2. The distilled water with low N_2 solubility, which was displaced by N_2, was flowing on its own. However, in the case of water displaced by CO_2 with the solubility of approximately 0.05－0.25 mol/kg, the displacement process was described as "the CO_2-H_2O solution flow".

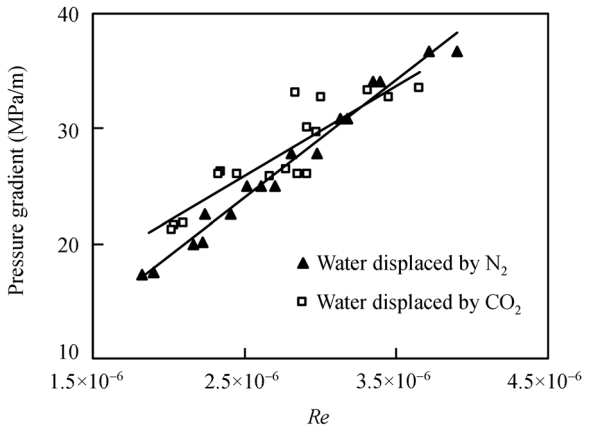

Figure 4 The pressure gradients influence on Reynolds numbers.

2.3 The corrosion of the CO_2-H_2O solution in cores

The influence of the corrosion reaction on the component changes of rock and clay minerals is shown in Tables 3 and 4.

The calcite content within the rock greatly decreased after the injection of CO_2-KCl saline water. A smaller decrease in potash feldspar content was also found. The calcite content for natural samples decreased from 23.7% (18-8-1) to 1.2% (18-8-5), and the potash feldspar content decreased from 23.8% to 12.2%. This occurred because CO_2 molecules (or carbonic acid when reacting with water) reacted with carbonate (or calcite) within the rock, yielding water soluble $Ca(HCO_3)_2$.

Table 5 shows that the average radius of pores and secondary pores were all enlarged, which demonstrated corrosion and pore enlargement effects at varying degrees. The results indicated that intergranualar pores of the synthetic core increased from 30－100 μm at the original range (PC-1) to 50－200 μm after the fluid was injected (PC-1#), while the natural core's intergranualar pores increased from 10－30 μm at the original range (18-8-1) to 30－100 μm (18-8-5). The secondary pore of the natural sample increased from 1－10 μm to 10－40 μm. This demonstrated that the effects of the corrosion reaction and the reaming effect during the CO_2-H_2O solution injection enhanced the core's permeability.

Under a pressure of 1.9 MPa, a saline solution of 1% KCl saturated with CO_2 was injected into cores. Ions in the outflow collected at different time-intervals were analyzed with ICP, as shown in Figure 5.

Table 3 Results of XRD lithology analysis before/after CO_2 injection

Samples	The species and contents of lithology (%)						The total amount of clay minerals (%)
	Q	K-F	P	C	P	S	
PC-1	67.3/67.3	0.5/0.5		0.6/0.6	–	–	31.6/31.6
18-8-1	15.0/28.5	23.8/12.2	26.3/30.1	23.7/1.2	–	–	11.2/28.0

Q, Quartz; K-F, K-feldspar; P, plagioclase; C, calcite; P, pyrite; S, siderite.

Table 4 Results of XRD mineral analysis before/after CO_2 injection

Samples	The relative content of clay minerals (%)						Mixed-layer ratio (% S)	
	S	I/S	I	K	C	C/S	I/S	C/S
PC-1		68/68	32/32				25/25	
18-8-1		83/76	1/1		16/23		25/20	

Table 5 Results of SEM analysis before/after CO_2 displacement

Samples	Analysis contents	Amplification
PC1-1	panorama, intergranular pores 30—100 μm, well connected	200
	intergranular flake I/S mixed-layers and dissolution pores	3000
	needle-like aragonite at the surfaces of grains and dissolution pores	8000
	calcite crystal and flake mixed-layer I/S in the secondary pores	3500
PC1-1#	panorama, loose packing, intergranular pores 50—200 μm, well connected	300
	mass microcrystalline calcite at the surfaces of grains	5650
	flake of illite, chlorite and flocculent mixed-layer I/S on the surfaces of grains	3580
	microcrystalline calcite at the surfaces and intergranular	955
18-8-1	panorama, dense packing, intergranular pores 10—30 μm, poor connected	300
	acicular-leaf chlorite covering the surfaces of grains	9220
	intergranula calcite cements	1680
	intergranula flake and filamentous illite and acicular-leaf chlorite	5260
	leaching feldspar, secondary pores 1—10 μm	1580
18-8-5	panorama, loose packing, intergranular pores 30—100 μm, well connected	300
	authigenic quartz crystal, flake and filamentous illite in intergranula	1870
	leaching feldspar, secondary pores 10—40 μm	907
	flake and filamentous illite and authigenic quartz crystal on the surfaces of grains	6270
	quartz overgrowth degree III, beehive mixed-layer I/S and bladed chlorite on the surfaces of grains	2980

Samples PC-1# and 18-8-5 were synthetic and natural cores after CO_2 corrosion, respectively.

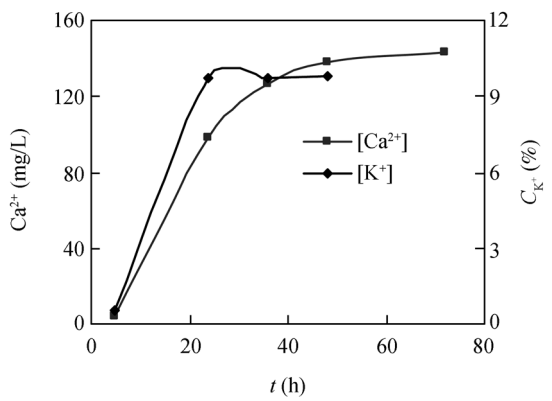

Figure 5 Ion concentration of effluent changes with time during injection process.

The concentration of [K^+] from the outflow reached its climax after 1 h, which equaled the value of [K^+] in standard saline water. The concentration of [Ca^{2+}] increased to a basically stable value after 40 h of injection, and reached its corrosion reaction dynamic equilibrium. However, the concentration of [Ca^{2+}] throughout the entire injection process was much lower than that of [K^+] because of the low corrosion reaction rate caused by carbonic acid formed after the dissolution of CO_2 in water. The weak acidic solution (pH≥2.8[18]) produced a low concentration of [HCO_3^-] and, in doing so, resulted in the uniform dissolution and corrosion.

2.4 The influence of the CO_2 solution on permeability

The flow rate of CO_2 at the outlet changed irregularly with a large fluctuation during the injection process when different CO_2 concentrations (or different CO_2 fractional pressures) of KCl solution were injected. The results based on a 10-day displacement indicated that permeability increased during the injection process under the CO_2 fractional pressure of 1.5 MPa, which confirmed the acidizing function of the CO_2-KCl solution. Unlike conventional acidizing systems, the weaker

acidic solution and faster diffusion of the CO_2 molecules within it led to improved acidizing uniformity throughout the entire reservoir. Together with its inhibition in a clay expansion, the possibilities of secondary pollution greatly reduced during the injection of CO_2, which was unlike other acidizing systems (Figure 6).

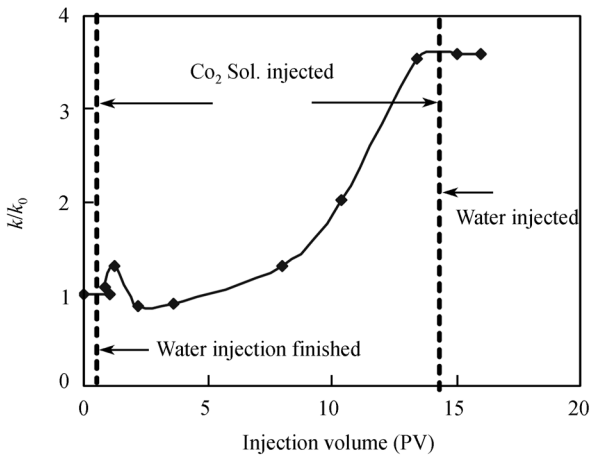

Figure 6 The injection volume of CO_2 solution influence on cores permeability.

3 Discussion of mechanisms

3.1 Microscale effect influence on percolation behavior

With the reduction of space, the scale effect on flow behavior became more apparent. When the difference between the effective flow radius of a fluid and pipe radius or the equivalent radius of flow space intensified to some extent, the influence of the wall adsorbent layer or the wall immobile layer caused the results to deviate from classical fluid mechanics. The scale effect includes not only the adsorbent layer thickness between the fluid and the solid wall, but also the characteristics of the adsorbent layer's diffusion and mass transfer.

Solid-liquid interface research is traceable back to the study of liquid wetting behavior on solid surfaces and such influence mechanisms as the Van der Waals model[19] which primarily involves the intermolecular interaction force. Salima Rafaï et al.[20] found that the thickness of liquid absorbent layers on solid surfaces varied from 1—30 nm through measurements of contact angle and surface free energy with an elliptically polarized light device.

Not only thickness but also structure and morphology of the wall absorbent layer changed with the physical and chemical reaction between fluids and solids. For example, there were three kinds of structures [21] for water in the interlayer between water and silicon dioxide, called "icelike" configuration (the first three layers, 0.5—1.0 nm), "transitional layer" between the completely self-associated network and a liquidlike configuration (0.8—1.5 nm), and "bulk liquid configuration" (1.2—3.0 nm).

Generally, liquids had much less molecular motion and incompressibility when compared with gases. With the increase of ambient pressure, the concentration of gas molecules on the surface adsorbed layer increased, and the adsorption manner on solid surfaces or pore spaces ranged from monolayers to multilayers and capillary condensation. These three stages coexisted because of the heterogeneity of solid surfaces (uneven surfaces or porous media)[20]. CO_2 had a lower viscosity and higher velocity at its conventional scale because its apparent viscosity was 0.83—0.84 times[21,22] that of N_2 under experimental conditions. Together with the reduction of flowing space, the microscale effect resulting from adsorption behavior and the interaction between fluids and solid walls led to much lower viscosity of CO_2 than that of N_2 and a much greater velocity in microtubes.

Additionally, the higher surface diffusibility of CO_2 in adsorption layers was another factor of the higher apparent permeability, and the effects of surface diffusion were neglected when the flow velocity of CO_2 exceeded 10^{-2} m/s.

CO_2 dissolved in aqueous solution enhanced not only diffusibility but also the diffusion coefficient of other components in the solution. The diffusion coefficient of methyl orange in water at 40℃ measured by Hori T[23] was 1.2×10^{-9} m^2s^{-1}, changing to 7.8×10^{-9} m^2s^{-1} under the same conditions except with a CO_2 fractional pressure of 21.1 MPa, measured by Michael A. Matthews[24]. Therefore it was apparent that the diffusion coefficient of methyl orange was enhanced with the admixture of CO_2.

The cause of the increase of apparent permeability of water after CO_2 was dissolved in it was due to the dissolution and higher molecular diffusibility of CO_2, such that the increase of molecular energy at the wall's adsorbent layer made a quantity of water molecules become mobile thereby reducing the thickness of the adsorbent layer in the microtube, which correspondingly

enlarged the effective flow radius of the CO_2 solution.

3.2 Pressure influences

For the flow of gas in microtubes or porous media, pressure greatly influences its flow behavior. Pressure influences the solubility of carbon dioxide in water as well as the flow behavior of water. All of the experiments on CO_2-H_2O flow in microtubes were carried out under pressures of not more than 1.5 MPa, which was far below the formation pressure. Thus there were greater differences between the CO_2-H_2O solution and pure H_2O. In summary, the increase of apparent permeability after dissolving CO_2 into the carbonate rock bearing formation was brought about by the corrosion and pore enlargement effect as well as by changes of solution characteristics. The latter resulted in enlargement of the effective flow radius, which increased its flow ability.

At present, most of the oil reservoirs in China yield oil mixed with water at the same layers. Therefore, it is necessary to consider reservoir environmental changes caused by the corrosion of carbonic acid formed after injecting CO_2 into reservoirs.

The results indicated that CO_2 had better injectivity than N_2. However, the diffusion properties and corrosion reactions between the CO_2-H_2O solution and rock could cause early breakthrough in reservoirs, which in turn influenced storage security[25] and oil displacement efficiency. Therefore, the results based on these experiments concerning the seepage characteristics of CO_2 and the physical chemical reactions between its aqueous solution and rock were useful for better understanding of both CO_2 flooding mechanisms and underground storage.

1 Klins M A. Carbon Dioxide Flooding: Basic Mechanisms and Project Design (Translated by Cheng S J)(in Chinese). Beijing: Petroleum Industry Press, 1989. 82－90
2 Zuo Y X, Stenby E H. A Linear gradient theory model for calculating interfacial tensions of mixtures. J Colloid Interf Sci, 1996, 182: 126－132[DOI]
3 Sun C Y, Chen G J. Measurement of interfacial tension for the CO_2 injected crude oil + reservoir water system. J Chem Eng Data, 2005, 50: 936－938[DOI]
4 Huang Y Z, Liu F H, Yang Z M. Mass transfer of complex chemical fluid in porous media. Acta Mech Sin (in Chinese), 2002, 34(2): 256－260
5 Yang Q, Nie M X, Song F Q. Threshold pressure gradient of low permeability sandstone. J Tsinghua Univ (Science and Technology) (in Chinese), 2004, 44(12): 1650－1652
6 Chen Y M, Zhou J, Liu W X, et al. Experimental demonstration of the non-darcy phenomenon during low velocity flow through porous media. J Chongqing Univ (Natural Science Edition) (in Chinese), 2000, 23(Suppl): 59－61
7 Liu J J, Liu X G, Hu Y R. Study on nonlinear seepage of rock of low permeability. Chin J Rock Mech (in Chinese), 2003, 22(4): 556－561
8 Karacan C O, Okandan E. Adsorption and gas transport in coal microstructure: Investigation and evaluation by quantitative X-ray CT imaging. Fuel, 2001, 80: 509－520[DOI]
9 Yu D, Jackson K, Harmon T C. Dispersion and diffusion in porous media under supercritical conditions. Chem Eng Sci, 1999, 54: 357－367[DOI]
10 Choi J G, Do D D, Do H D. Surface diffusion of adsorbed molecules in porous media: Monolayer, multilayer, and capillary condensation regimes. Ind Eng Chem Res, 2001, 40: 4005－4031[DOI]
11 Cicero G, Grossman J, Catellani A, et al. Water at a hydrophilic solid surface probed by *ab initio* molecular dynamics: Inhomogeneous thin layers of dense fluid. J Am Chem Soc, 2005, 127: 6830－6835[DOI]
12 Asay D B, Kim S H. Evolution of the adsorbed water layer structure on silicon oxide at room temperature. J Phys Chem B, 2005, 109: 16760－16763[DOI]
13 Li K, Horne R N. Gas slippage in two-phase flow and the effect of temperature. SPE 68778
14 Rushing J A, Newsham K E, Van Fraassen K C. Measurement of the Two-Phase Gas Slippage Phenomenon and Its Effect on Gas Relative Permeability in Tight Gas Sands. SPE 84297
15 Li Z H, Zhou X B, Zhu S N. Flow characteristics of non-polar organic liquids with small molecules in a microchannel. Acta Mech Sin (in Chinese), 2002, 34(3): 432－437
16 Xu S L, Yue X A, Hou J R. Experimental investigation on flow characteristics of deionized water in microtubes. Chin Sci Bull, 2007, 52(1): 120－124
17 Liu J J, Liu X G. The effect of effective pressure of porosity and permeability of low permeability porous media. J of Geomech (in Chinese), 2001, 7(1): 41－44
18 Toews K L, Shroll R M, Wai C M, et al. PH-defining equilibrium between water and supercritical CO_2 influence on SFE of organics and metal chelates. Anal Chem, 1995, 67: 4040－4043[DOI]
19 Cahn J W. Critical point wetting. J Chem Phys, 1977, 66(8): 3667－3672
20 Rafaï S, Bonn D, Bertrand E, et al. Long-range critical wetting: Observation of a critical end point. Phys Rev Lett, 2004, 92(24): 1－4[DOI]
21 Seibt D, Vogel E, Bich E, et al. Viscosity measurements on nitrogen. J Chem Eng Data, 2006, 51: 526－533[DOI]
22 Iwasaki H, Takahashi M. Viscosity of carbon dioxide and ethane. J Chem Phys, 1981, 74(3): 1930－1943[DOI]
23 Hori T, Rohner R M, Kojima H, et al. Structure correlation between ciffusion coefficients of simple organic compounds and of anionic and cationic dyes in water. J Soc Dyers Colour, 1987, 103: 265－270
24 Matthews M A, Becnel J M. Diffusion coefficients of methyl orange in dense carbon dioxide with the micelle-forming surfactant dehypon Ls-54. J Chem Eng Data, 2003, 48: 1413－1417[DOI]
25 Zeng R S, Sun S, Chen D Z, et al. Decrease carbon dioxide emission into the atmosphere-underground disposal of carbon dioxide. Bull Nat Nat Sci Found Chin (in Chinese), 2004. 196－200